Creutzfeldt, B., Güntner, A., Thoss, H., Merz, B., Wziontek, H. (2010): Measuring the effect of local water storage changes on in-situ gravity observations: Case study of the Geodetic Observatory Wettzell, Germany. - Water Resources Research, 46, W08531

DOI: 10.1029/2009WR008359

Measuring the effect of local water storage changes on in situ gravity observations: Case study of the Geodetic Observatory Wettzell, Germany

Benjamin Creutzfeldt,[1] Andreas Güntner,[1] Heiko Thoss,[1] Bruno Merz,[1] and Hartmut Wziontek[2]

Received 6 July 2009; revised 13 January 2010; accepted 16 February 2010; published 17 August 2010.

[1] Local water storage changes (WSC) are a key component of many hydrological issues, but their quantification is associated with a high level of uncertainty. High precision in situ gravity measurements are influenced by these WSC. This study evaluates the influence of local WSC (estimated using hydrological techniques) on gravity observations at the Geodetic Observatory Wettzell, Germany. WSC are comprehensively measured in all relevant storage components, namely groundwater, saprolite, soil, topsoil, and snow storage, and their gravity response is calculated. Total local WSC are derived, and uncertainties are assessed. With the exception of snow, all storage components have gravity responses of the same order of magnitude and are therefore relevant for gravity observations. The comparison of the total gravity response of local WSC to the gravity residuals obtained from a superconducting gravimeter shows similarities in both short-term and seasonal dynamics. A large proportion of the gravity residuals can be explained by local WSC. The results demonstrate the limitations of measuring total local WSC using hydrological methods and the potential use of in situ temporal gravity measurements for this purpose. Nevertheless, due to their integrative nature, gravity data must be interpreted with great care in hydrological studies.

Citation: Creutzfeldt, B., A. Güntner, H. Thoss, B. Merz, and H. Wziontek (2010), Measuring the effect of local water storage changes on in situ gravity observations: Case study of the Geodetic Observatory Wettzell, Germany, *Water Resour. Res.*, *46*, W08531, doi:10.1029/2009WR008359.

1. Introduction

[2] Until now, local water storage changes (WSC) have been considered as only measurable on the point scale (e.g., piezometer wells, soil moisture probes), but they are a key component in catchment characterization [*Kirchner*, 2009]. High precision in situ gravity measurements are influenced by local WSC in groundwater, soil moisture, snow, or surface water storage. Gravity observations may be used for hydrological modeling, because many hydrological models are based on the water balance equation; they are generally run with input fluxes, and the system parameters are calibrated to match the outflow fluxes. Permanent gravity observations provide information about system changes and may be used as an additional calibration parameter. For example, *Werth et al.* [2009] calibrated a global hydrological model against runoff and global gravity variations using a 2-D calibration scheme.

[3] Many different studies have highlighted the relationship between local WSC and in situ gravity measurements, for example, for removing the "hydrological noise" from gravity observations [e.g., *Bower and Courtier*, 1998; *Crossley et al.*, 1998; *Virtanen*, 2001], for comparing the signal with the results from the GRACE satellite gravity mission [e.g., *Crossley et al.*, 2003; *Llubes et al.*, 2004; *Neumeyer et al.*, 2008], for studying hydrological processes, or for deriving hydrological parameters. In groundwater studies, time lapse gravity measurements in conjunction with pump tests or groundwater table fluctuations are used to estimate in situ the specific storage coefficient [e.g., *Gehman et al.*, 2008; *Pool and Eychaner*, 1995]. In the study by *Hokkanen et al.* [2006], the fracture gaps and the porosity were used as a calibration parameter. *Van Camp et al.* [2006] used soil moisture measurements to calculate the gravity effect of soil moisture, using the block content of the soil as a calibration factor. *Jacob et al.* [2009] used the gravity measurement to derive the apparent porosity in the vadose zone.

[4] Recently, the focus has been on the combination of spatially semidistributed hydrological models and gravity observations. *Hasan et al.* [2008] calibrated a lumped soil moisture storage model and a hillslope storage Boussinesq model for the groundwater against runoff and in situ gravity signals. *Naujoks et al.* [2010] used a hydrological model based on hydrological response units. The derived hydrological masses were spatially distributed according to a geophysical underground model and finally compared to the gravity data.

[5] In spite of these promising results, the hydrological effect is still the least understood signal component in

[1]Section of Hydrology, German Research Centre for Geosciences, Potsdam, Germany.
[2]Section of National Reference Systems for Gravity, Federal Agency for Cartography and Geodesy, Frankfurt, Germany.

0043-1397/10/2009WR008359

gravity measurements. After correcting the integral gravity signal for comparatively well-known effects of polar motion, ocean, and Earth tides and atmospheric mass variations, the remaining signal (the gravity residuals) is considered to be caused mainly by WSC. Besides the influence of local water masses by Newtonian attraction, the deformation of the Earth's crust and the Newtonian attraction due to large-scale water storage variations also influence the gravity residuals. In the case of the Geodetic Observatory Wettzell, Germany, local WSC can contribute up to tens of μGal to the gravity residuals [*Creutzfeldt et al.*, 2008], while the influence of large-scale WSC is about one order of magnitude smaller [*Wziontek et al.*, 2009b].

[6] The influence of local WSC (attraction), large-scale storage changes (attraction and deformation), and other non-hydrology-related mass effects on in situ gravity observations needs to be defined before (1) using superconducting gravimeters (SGs) as a measurement tool for small-scale hydrological studies, (2) comparing local gravity observations with global gravity observations such as those from the GRACE satellite mission, and (3) studying geodynamic phenomena based on gravity data such as postglacial rebound or oscillations of the Earth's core (e.g., Slichter modes). Because the influence of local WSC is considered to be the major part of the SG residuals, this study will focus on the estimation of local hydrological masses and the corresponding gravity response.

[7] As pointed out by *Gettings et al.* [2008], *Jacob et al.* [2008], or *Naujoks et al.* [2010], it is necessary to consider all relevant hydrological water storage components in local studies. As highlighted by *Pool* [2008], focusing on only one storage component may lead to an incorrect result. We are not aware of a study that has measured all possible water storages and compared them to the gravity signal.

[8] In this study, we monitor all different local water storage components using hydrological measurement techniques, and we determine their effect on in situ gravity observations. In order to avoid integrating information that may not originate from local WSC, it is essential to exclude any calibration against the SG signal when estimating the local WSC from the observations. We therefore apply a purely observation-based approach to the SG at the Geodetic Observatory Wettzell, Germany, the site we selected for our study.

[9] For this site, *Creutzfeldt et al.* [2008] showed that between 52% and 80% of the local hydrological gravity signal is generated within a radius of 50 m around the SG. The higher percentages apply to situations where WSC occur closer to the terrain surface, meaning that soil moisture has a smaller sphere of influence than groundwater. About 90% of the signal is generated in an area within a radius of around 1000 m. Therefore, within the scope of this study, we focus on the direct vicinity of the SG Wettzell and on water (re-)distribution over depth. We assume that for this small radius of influence the variability of the hydrological state variables and their gravity effect are more pronounced over depth than over area. Following this assumption, we explicitly resolve the variability over depth in a 1-D approach. The unresolved spatial variability is recognized partially in a simple uncertainty analysis based on observation data. We pursue this 1-D approach by focusing separately on each storage component, namely snow (section 3), soil moisture (section 4, unsaturated zone), groundwater (section 5, saturated zone), and saprolite water (section 6, unsaturated zone). Processing of the SG data, calculation of the gravity response due to the WSC, and the comparison are described in section 7. Finally, we discuss the different sources of uncertainty and the potential applications/limitations of the hydrological use of SG measurements.

2. Study Area

[10] The Geodetic Observatory Wettzell, operated by the Federal Agency for Cartography and Geodesy (BKG), is located on a mountain ridge in the southeast of Germany [*Schlüter et al.*, 2007]. Around the SG, we mapped the topography using differential GPS (DGPS) and created a digital elevation model (DEM) by merging 14,000 DGPS measurements and an existing DEM with a cell size of 10 m and a mean height accuracy of 1 m (see Figure 1).

[11] The study area is characterized by a temperate climate with a mean annual precipitation of 863 mm, a potential evapotranspiration (according to *Haude* [1955]) of 403 mm, and a mean annual temperature of 7°C (climate station Höllenstein-Kraftwerk, 1947–2005). The hydrologically relevant climate parameters (air temperature, relative humidity, wind, precipitation, snow, global radiation, and net radiation) are measured at the Observatory Wettzell. Data gaps were filled with data of climate station 127 Allmannsdorf (distance ~6 km) [*LfL*, 2009]. For the study period between 18 July 2007 and 31 March 2009, precipitation amounted to 1390 mm and the average air temperature was 7.75°C. All data used in this study are processed to 1 h intervals.

[12] The area around the SG Wettzell is rural, characterized by a mosaic of grassland and forest. The immediate surroundings of the SG Wettzell are dominated by grassland. The geology consists of acidic metamorphic rocks (Biotite-Gneiss). In general, this basement zone merges seamlessly with a fractured zone, followed by a saprolite cover consisting mainly of Grus (weathered Gneiss). The saprolite can be covered by a periglacial weathering cover [*Völkel*, 1995].

[13] The SG Wettzell is positioned near ground level and is based on a concrete foundation with a size of 1.4 × 1.4 × 1.2 m (width × depth × height) in a building with a length of 9.7 m and a width of 5.7 m. The base plate has a thickness of 0.3 m, and precipitation from the SG roof is drained away through a tank ~20 m from the SG [*Creutzfeldt et al.*, 2008].

[14] The underground was characterized using undisturbed and disturbed soil samples from two different boreholes and three different soil pits (Figure 2). The soil samples were analyzed in the laboratory: (1) the grain size distribution was estimated by sieving and through the sedimentation method, (2) the organic matter by the loss-on-ignition method with a muffle furnace, (3) the bulk density by weight and volume of the sample, (4) the particle density with a gas pycnometer, and (5) the porosity from the bulk and particle density. On the basis of these results and hydrological instrumentation techniques, the underground is characterized and classified into different geological zones that are related to the following hydrological storage components: (1) the topsoil storage (0.0–0.3 m), (2) the soil storage (0.3–1.25 m), (3) the saprolite storage (1.25–11.0 m), and (4) the groundwater zone (11.0–19.0 m) (see Figure 2 and Table 1). In this study, "groundwater zone" refers to the saturated subsurface zone where water is free to move under the influence of gravity and is associated with the fractured zone. The three other storages belong to the vadose

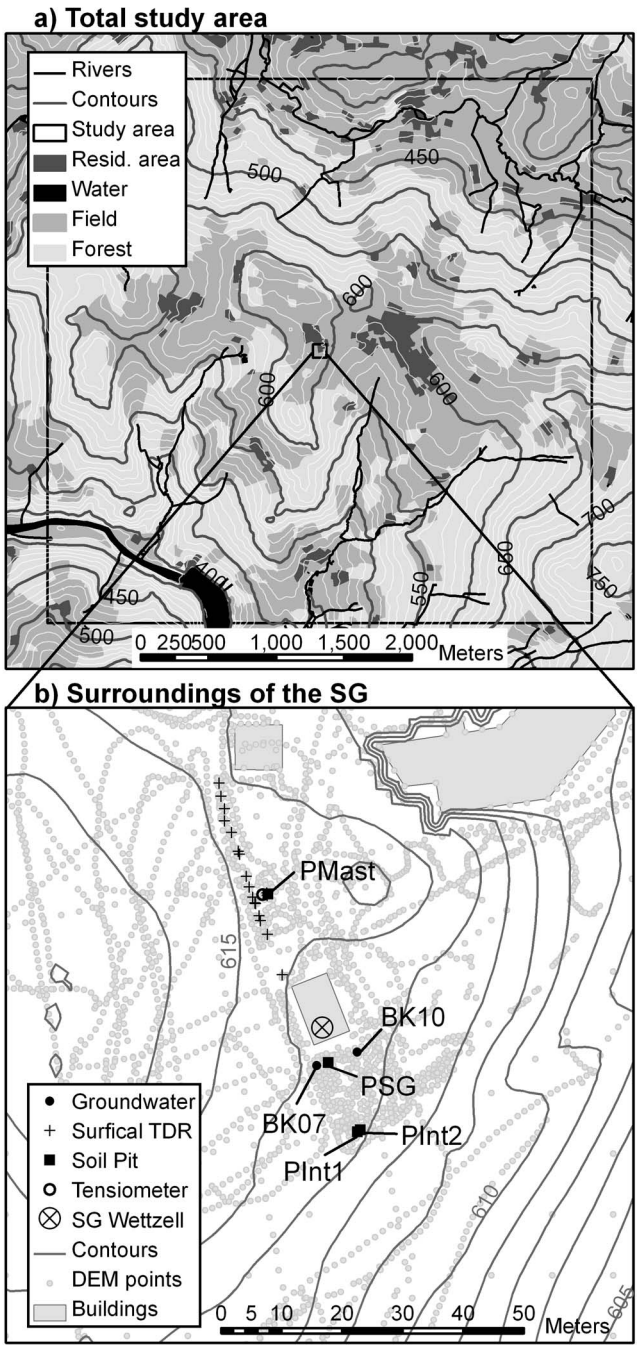

Figure 1. (a) Map of the total study area with land use classification [*BKG*, 2005], rivers, and contour lines (contour distance 50 m (dark gray) and 10 m (light gray)). (b) Map of the surroundings of the SG with hydrological sensors, DGPS measurement points, and contour lines (contour distance, 1 m).

zone where the water flow is mainly controlled by gradients of the capillary potential.

3. Snow Storage

[15] The snow mass and height are measured using a snow monitoring system consisting of a snow pillow and an ultrasonic distance sensor [*Sommer*, 2007, 2008]. The snow pillow measures the snow load (the snow water equivalent) using a pressure transducer, and the ultrasonic sensor measures the snow depth. The snow height record was inspected visually, and clear outliers were replaced with adjacent interpolated measurements. Snow water equivalent values were only allowed if the snow height was greater than zero because the snow pillow measurements are influenced by

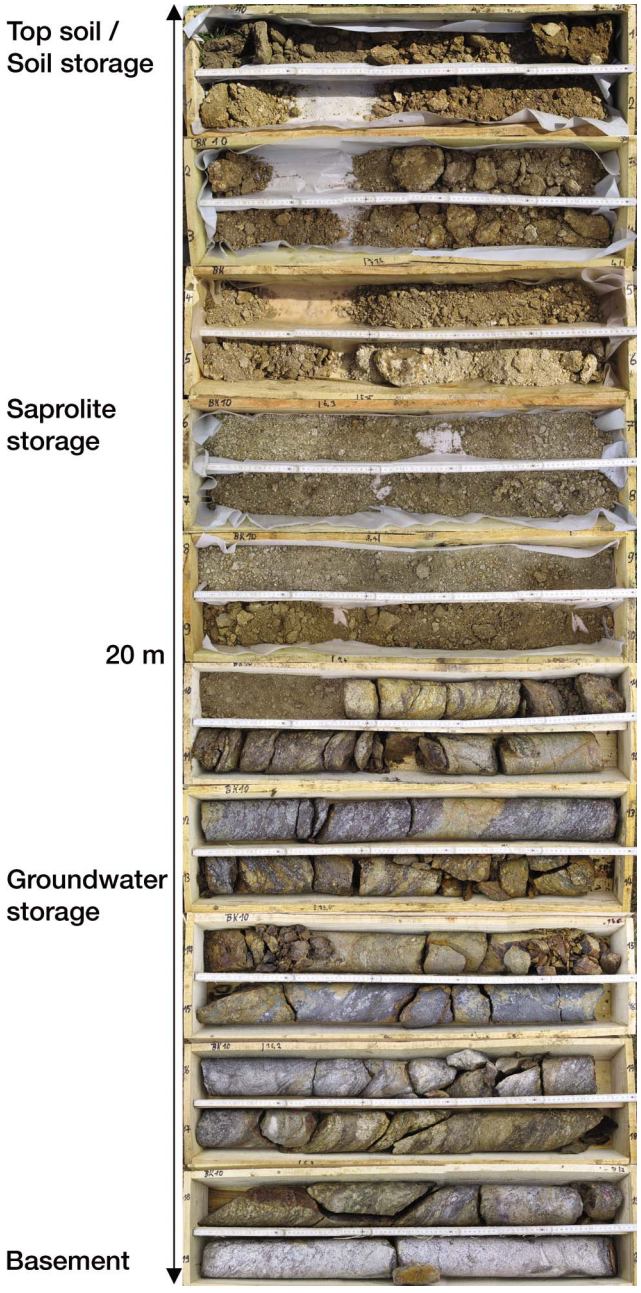

Figure 2. Core of borehole BK10 and the corresponding hydrological storage components: (1) the topsoil storage (0.0–0.3 m), (2) the soil storage (0.3–1.25 m), (3) the vadose saprolite storage (1.25–11.0 m), and (4) the saturated groundwater zone (11.0–19.0 m). Note that the abrupt transition in the depth of ~10 m is due to a change in the drilling technique from pile-driving to diamond core drilling (length of one core box is 1 m).

Table 1. Physical Characteristics of the Different Hydrological Storage Components[a]

Parameter	Unit	Top Soil Storage	Soil Storage	Saprolite Storage	Groundwater Storage
Description	–	Ap horizon	IIBv/IIIfBt/IVCv horizon	Saprolite	Fractured zone
Depth	m	0.00–0.30	0.30–1.25	1.25–11.00	11.00–19.00
Organic matter	%	5.30 ± 0.69 (3)	4.29 ± 1.75 (3)	–	–
Gravel (>2000 μm)	%	6.97 ± 1.59 (3)	3.08 ± 1.65 (3)	14.40 ± 7.74 (22)	–
Sand (>63 μm)	%	53.50 ± 7.70 (3)	57.15 ± 11.45 (3)	80.49 ± 2.92 (22)	–
Silt (>2 μm)	%	26.61 ± 5.91 (3)	24.80 ± 7.60 (3)	17.29 ± 2.63 (22)	–
Clay (<2 μm)	%	14.59 ± 2.66 (3)	13.76 ± 2.51 (3)	1.96 ± 0.95 (22)	–
Bulk density	g/cm^3	1.43 ± 0.15 (19)	1.53 ± 0.14 (30)	1.75 ± 0.27 (35)	–
Porosity	m^3/m^3	0.46 ± 0.06 (19)	0.42 ± 0.05 (30)	0.34 ± 0.10 (35)	–

[a]Numbers of samples in brackets.

seasonal temperature variations due to the expansion of trapped air bubbles in the water-glycol mixture of the snow pillow. Figure 3 shows the time series of the snow height and snow water equivalent. Nearly no snow was observed during the winter of 2007–2008. On 27 February 2009, a maximum snow height of around 656 mm and a corresponding snow water equivalent of 75 mm were measured. From here, snowmelt started and lasted until 16 March 2009.

4. Top Soil and Soil Storage

[16] The soil is made up of gravelly sandy loamy brown soils (Cambisols), with an Ap/IIBv/IIIfBt/IVCv horizon sequence in the immediate vicinity of the SG. The topsoil moisture between 0.0 and 0.3 m was measured by 18 0.3 m long 3-rod time domain reflectometry (TDR) probes. Soil moisture between 0.3 and 2.0 m depth was monitored in three different soil pits (PSG, PMast, and PInt). PSG and PMast consisted of TDR probes at depths of 0.3, 0.4, 0.6, 1.0, 1.5, and 2.0 m and had a distance to the SG of 6 and 17 m, respectively. PInt comprised two TDR profiles (PInt1 and PInt2) at a distance of 17 m to the SG and of 1 m to each other (Figure 1). In this soil pit, soil moisture was measured at 0.3, 0.4, 0.6, 1.0, and 1.5 m. 0.075 m long 3-rod TDR probes were used for all TDR profiles.

[17] All TDR probes were connected to TDR100 time domain reflectometers, and data were generally logged every 15 min by a CR1000 System [*Campbell Scientific Inc.*, 2008, 2009]. The soil moisture was calculated from the dielectric permittivity using the Topp equation [*Topp et al.*, 1980], as this approach is suitable for loamy sandy soils and can be expected to be accurate enough, especially if one is mainly interested in the relative soil moisture changes as is the case in our study [*Roth et al.*, 1992]. Each time series was inspected visually, and clearly anomalous measurements caused by incorrect analysis of the TDR waveform were removed. The data were resampled to 1 h intervals using a smoothing algorithm. Due to short circuiting of the PMast probe at 1.0 m depth during installation, the probe was removed from further analysis.

[18] The topsoil moisture variation is illustrated in Figure 4a, and the soil moisture variation at different depths in Figures 4b–4f. Temporal variations in soil moisture correspond well between all sensors. The offset in absolute values of PSG 0.6 m (Figure 4c) and the deviation at a depth of 1.5 m (Figure 4e) of the different TDR profiles may be due to different soil material or installation problems. Such offsets were not corrected in this study because we focused on the relative temporal change of water storage.

[19] The upper sensors exhibit more pronounced weather-related variations than the lower ones. We can clearly identify a drying period of the soil in the summer of 2008 and a wetting front from the top in autumn. In summer and autumn of 2008, a decline of soil moisture occurred below 1.0 m, implying that only little percolation occurs below this zone. The moisture decline for profile PInt is not as pronounced as for the other profiles, probably due to the higher clay/silt content. On 31 July 2008, the dry period ended with a heavy rainfall event of ~60 mm/2 h, reflected by a sharp increase of soil moisture. The very fast reaction of some probes up to a depth of 1.5 m indicates the activation of macropores as preferential flow paths. These macropores are most likely an immanent property of the soil, because the TDR probes were installed 0.1 m away from the soil pit wall in undisturbed soil. Also, the soil in the soil pit was highly compacted after installation so that artificial flow paths to the probes are not likely to exist. During winter (December 2007 to January 2008 and December 2008 to March 2009), markedly lower apparent soil moisture values measured at up to 0.4 m (Figures 4a and 4b) do not reflect a real decrease of soil water content but are due to soil freezing as confirmed by soil temperature measurements. The TDR system records the change in soil dielectric permittivity due to the change of the aggregate state of water. Observed soil temperature values indicate that, below a depth of 0.4 m, a real decrease of soil moisture

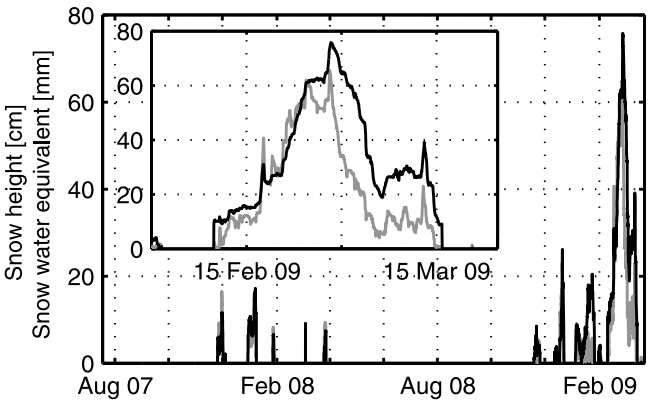

Figure 3. Seasonal variation of snow height (gray line) and snow water equivalent (black line) for the whole study period and for the snow event during February/March 2009.

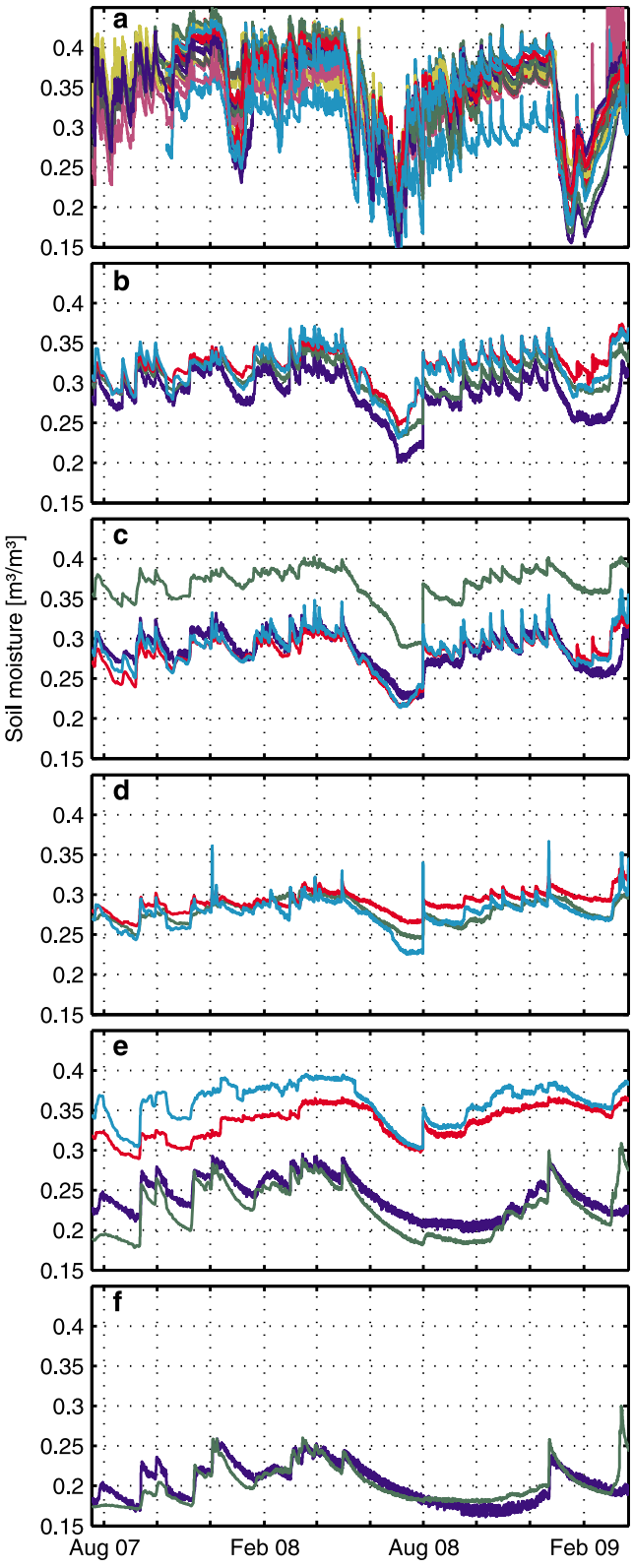

Figure 4. Soil moisture variation in different depths. (a) Top soil moisture variations from 0.0 to 0.3 m measured by 18 different TDR probes (different colored lines). Soil moisture variation at depths of (b) 0.4 m, (c) 0.6 m, (d) 1.0 m, (e) 1.5 m, and (f) 2.0 m measured by four TDR profiles: PMast (blue line), PSG (green), PInt1 (red), and PInt2 (turquoise).

may be due to cryosuction [*Hohmann*, 1997] caused by the frozen near-surface soil horizons.

5. Groundwater Storage

[20] The aquifer around the Geodetic Observatory Wettzell is unconfined and is characterized by high heterogeneity. Groundwater is usually associated with the fractured zone but may extend to the saprolite zone. The water table is highly variable over time and space. In different groundwater wells at the observatory, the water table depth varies between 4 and 15 m. It can show seasonal fluctuations as high as 4 m and a quick response to single rainfall events.

[21] Groundwater table, electrical conductivity, and temperature are monitored with multiparameter sensors [*SEBA*, 2008] (Figure 5) in the boreholes close to the SG (Figure 1). The mean water table depth is 13.38 m (BK07) and 13.14 m (BK10) below ground surface. The groundwater table variations of both wells show a seasonal course and are very similar (correlation coefficient, 0.9985). The seasonal amplitude amounts to 2.8 m. The steep rise in the groundwater table of ~2.2 m from 6 to 20 March 2009 is caused by snowmelt water (see also Figure 3).

[22] From 11 June 2008 0700 h to 13 June 2008 0900 h (Central European Time), a pump test was conducted to estimate the specific yield and to investigate the influence of the pump test on the SG measurements. In total, ~12.3 m^3 water were pumped from BK07, which corresponds to a constant pumping rate of 0.07 L/s. The water was drained into the sewerage 60 m away from the SG. The drawdown and the recovery of the water table after the pump was deactivated were measured in the pumping well and in the observation well (see also Figure 11).

[23] The analysis of the pump test is based on the methods summarized by *Kruseman and de Ridder* [1990] and *Langguth and Voigt* [1980]. On the basis of the two bore cores (BK07 and BK10), we set up a simplified hydrogeological model, assuming a homogeneous, isotropic, and unconsolidated aquifer (highly fractured Gneiss). The aquifer basement is estimated to be at a depth of 19 m, and hence, the aquifer thickness is about 7 m and the pumping well fully penetrates the aquifer. The time-drawdown curve did not show the phenomenon of a delayed water table response. Therefore, we can analyze the pump test using the method suggested by *Cooper and Jacob* [1946] and *Theis* [1935], applying a correction of the displacement data using the approach of *Jacob* [1944]. Both approaches were used to estimate the transmissivity (T), the saturated hydraulic conductivity (K_s), and the storativity (S) from the drawdown and recovery data, taking into account that these approaches are only valid under the assumptions listed above and by *Kruseman and de Ridder* [1990]. The straight line method is valid because the precondition that $t \geq 3.8(S/T)r^2$ applies to the pump test, where r is the radial distance between pumping and observation well (m) and t is the pump duration (h) [*TGL*, 1974]. The results of the pump test are presented in Table 2.

[24] In unconfined aquifers, the storativity is essentially equal to the specific yield (S_Y), which refers to the drainable porosity. The estimated specific yield ranges from 6.30×10^{-3} to 1.61×10^{-2} and is in line with literature values for fractured igneous rocks [e.g., *Maréchal et al.*, 2004]. For the fractured zone of the Bavarian Forest, *Rubbert* [2008] esti-

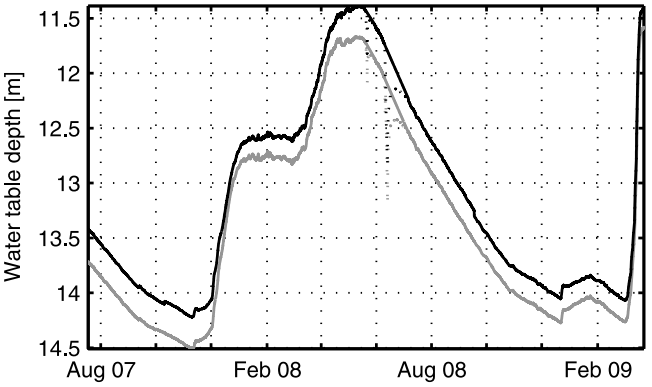

Figure 5. Water table depth variations of the two monitoring wells BK07 (gray line) and BK10 (black line). Dotted lines are raw and solid lines pump test corrected data.

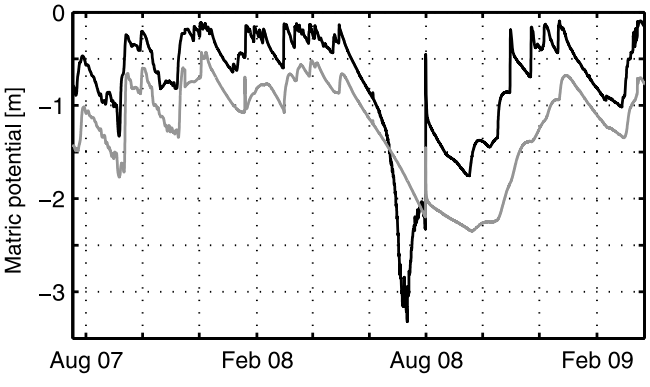

Figure 6. Seasonal variation of matric potential measured by tensiometers in ~1.0 (black line) and ~1.4 m depth (gray line).

mated the specific yield to range between 5×10^{-4} and 2×10^{-2}. Assuming that during the snowmelt event in February/March 2009 all water stored in the snow cover (75 mm) flows into the groundwater storage and causes a water table rise of 2.2 m there, S_Y can be estimated to be 3.41×10^{-2}. This value reflects the upper boundary for S_Y, because it is likely that not all snow water reaches the groundwater. For example, surface runoff or accumulation of snow water in the vadose zone can also occur.

[25] Depending on the method used, hydraulic conductivity varies from 7.07×10^{-3} to 1.40×10^{-2} m/h. Assuming steady state flow conditions at the end of the pump test, the hydraulic conductivity was estimated at 2.93×10^{-2} m/h based on Thiem's method. These values are of the same order of magnitude and correspond to the hydraulic conductivity values of the Upper Palatinate–Bavarian Forest region [*Büttner et al.*, 2003; *Rubbert*, 2008]. *Raum* [2002] conducted tracer experiments about 1 km away from the study area. He estimated that the "maximum distance velocity (v_{max})" for six different flow paths ranges between 1.83×10^{-1} and 1.52×10^{1} m/h. Assuming that the mean distance velocity is half of v_{max}, we can estimate K_s based on the hydraulic gradient and the estimated mean specific yield to range from 1.36×10^{-2} to 9.74×10^{-1} m/h. These values are one magnitude greater than the estimated hydraulic conductivity and represent the upper range of the estimated K_s values since these are derived from v_{max}.

6. Saprolite Storage

[26] The saprolite zone consists mainly of Grus (weathered Gneiss) at depths between 1.3 and 11.0 m (see Figure 2). This is generally a zone of high heterogeneity [*Rubbert*, 2008], including quartz veins and float blocks.

[27] Direct measurements of WSC were not possible because the high rock content (Table 1) and float blocks prevent the installation of soil moisture probes, access tubes, or soil pits in this zone. We therefore estimated the WSC in the saprolite zone $\Delta S_{Saprolite}$ (m/h) by estimating the upper and lower boundary flux

$$\Delta S_{Saporlite} = q_P - q_R \tag{1}$$

where the deep percolation q_P (m/h) refers to the water flux from the soil to the saprolite storage and the groundwater recharge q_R (m/h) is the flux from the saprolite to the groundwater storage.

6.1. Deep Percolation

[28] For the estimation of the upper boundary flux (the deep percolation flux q_P (m/h)), we used the Buckingham-Darcy law [*Buckingham*, 1907]

$$q_p = K(h)\left(\frac{dh}{dz} + 1\right) \tag{2}$$

where $K(h)$ is the hydraulic conductivity (m/h), h is the matric pressure head (m), and z is the vertical distance. The matric pressure head gradient dh/dz is estimated from tensiometer measurements at depths of ~1.0 and ~1.4 m (TS1 tensiometers, manufactured by UMS Munich). The tensiometer measurements started on 15 November 2007 (Central European Time) 1500 h. Between 18 July and 15 November 2007, matric pressure head values were derived from TDR measurements at the appropriate depth using the van Genuchten relationship derived from the tensiometers and TDR measurements. Figure 6 shows the time series for the tensiometer observations. The dry period of

Table 2. Aquifer Parameters Estimated From a Pump Test by Analyzing Drawdown and Recovery Data

	Jacob Straight Line Method		Theis Method		
Parameter	Drawdown	Recovery	Drawdown	Recovery	Mean
T (m^2/h)	9.77×10^{-2}	8.57×10^{-2}	4.95×10^{-2}	6.99×10^{-2}	7.57×10^{-2}
S_Y (−)	6.30×10^{-3}	6.86×10^{-3}	1.61×10^{-2}	9.15×10^{-3}	9.61×10^{-3}
K_s (m/h)	1.40×10^{-2}	1.22×10^{-2}	7.07×10^{-3}	9.98×10^{-3}	1.08×10^{-2}

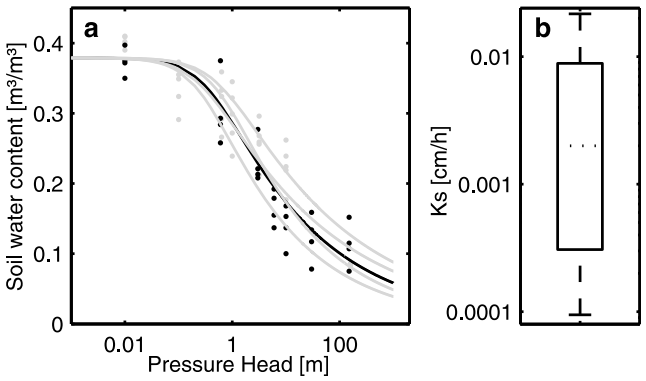

Figure 7. (a) Measured water retention data using borehole (black dots) and soil pit (gray dots) samples. Black line is the predicted van Genuchten model, and gray lines are the model variations. (b) Box plot of the measured saturated hydraulic conductivity (see Table 4) (dashed line, median; black box, lower and upper quartile; whiskers, lower and upper extreme values within 1.5 times the interquartile range).

the summer of 2008 is associated with a strong decline in the matric pressure head. On 31 July 2008, a steep rise in the matric pressure head is caused by a heavy rainfall event of around 60 mm within 2 h.

[29] The estimation of $K(h)$ is based on the Mualem-van Genuchten model [*Mualem*, 1976; *van Genuchten*, 1980], where the hydraulic conductivity is computed as

$$K(h) = K_s S_e^l \left[1 - \left(1 - S_e^{\frac{n}{(n-1)}}\right)^{1-\frac{1}{n}}\right]^2 \quad (3)$$

where S_e is the effective saturation

$$S_e = \frac{\theta(h) - \theta_r}{\theta_s - \theta_r} \quad (4)$$

and $\theta(h)$ is the water retention curve

$$\theta(h) = \theta_r + \frac{\theta_s - \theta_r}{[1 + |\alpha h|^n]^{1-\frac{1}{n}}} \quad (5)$$

[30] The parameter l is the pore connectivity, in this study assumed to be 0.5 [*Mualem*, 1976]. The parameter α is the inverse of the air entry pressure (cm^{-1}), n is the pore size distribution index, and θ_r and θ_s are the residual and the saturated water content, respectively (m^3/m^3).

[31] All van Genuchten parameters were derived by fitting the water retention curve to water retention data, which were estimated using undisturbed soil samples obtained during drilling (number of samples: 4, depth: 1.1–6.1 m) and from the soil pit PMast (number of samples: 5, depth: 0.6–1.4 m) (see Figure 7). The influence of each sample on the predicted parameter set was assessed by successively excluding one sample after another and fitting the retention curve to the remaining water retention data. The mean and the standard deviation are calculated from these nine different realizations, assuming a normal distribution of the four parameters. Finally, four different scenarios were modeled by calculating, the mean μ plus and minus 2 times the standard deviation σ for parameters α and n, resulting in a total of four permutations of α and n (Table 3).

Table 3. Predicted Parameters, Mean, and Standard Deviation of the van Genuchten Models

Parameter	θ_r	θ_s	α	n
Predicted	0.00	0.38	2.64	1.23
Mean	0.00	0.38	2.63	1.24
Standard Deviation	0.01	0.00	0.50	0.02
$\mu + 2\sigma$	0.01	0.38	3.63	1.28
$\mu - 2\sigma$	–	0.38	1.63	1.20

[32] We estimated the saturated hydraulic conductivity K_s from nine core samples (depth: 1.10–6.35 m) and eight samples from the soil pit PMast (depth: 0.6–1.4 m). Additionally, we measured in situ 15 K_s values with a constant head well permeameter at different depths ranging from 0.6 to 2.2 m. Figure 7 and Table 4 show the measured K_s values. The estimated K_s values vary over several orders of magnitude. Four measurements were identified to be influenced by macropore flow and were removed from further analysis. The Buckingham-Darcy approach considers only soil matric flow, and we assume that all other K_s values stand for flow in the soil matrix. We combined all samples from the different measurement techniques to increase the sample size because no significant differences could be observed between the different sample/measurement techniques. The distribution of K_s tends to show a non-Gaussian distribution (see Figure 7b), so we chose the median as a robust estimator and calculated the median of K_s to be 2.00×10^{-3} m/h. This value is within the range of the estimated K_s of the weathered zone [*Rubbert*, 2008] but is one magnitude lower than the K_s for the soil texture Sl3 (mean bulk density) of 1.75×10^{-2} m/h or for Su2 (high bulk density) of 2.67×10^{-2} m/h according to the German Institute for Standardization [*DIN*, 1998].

[33] The deep percolation is calculated based on equation (2) using the predicted van Genuchten model, the median K_s value and time series of the tensiometers. For the German hydrological year of 2008 (1 November 2007 to 31 October 2008), the deep percolation amounts

Table 4. Measured Hydraulic Conductivity Values[a]

	Soil Pit PMast	Drilling	Permeameter
	7.92×10^{-4}	1.09×10^{-4}	9.44×10^{-5}
	1.54×10^{-3}	1.73×10^{-4}	2.21×10^{-4}
	2.92×10^{-3}	2.50×10^{-4}	2.54×10^{-4}
	4.54×10^{-3}	3.02×10^{-4}	3.13×10^{-4}
	7.67×10^{-3}	1.01×10^{-3}	1.08×10^{-3}
	1.01×10^{-2}	1.56×10^{-3}	2.00×10^{-3}
	1.13×10^{-2}	2.00×10^{-3}	3.44×10^{-3}
	1.35×10^{-2}	2.15×10^{-3}	5.63×10^{-3}
		2.60×10^{-1}[b]	1.68×10^{-2}
			1.75×10^{-2}
			1.81×10^{-2}
			2.17×10^{-2}
			1.14×10^{-1}[b]
			1.70×10^{-1}[b]
			4.24×10^{-1}[b]
Count	8	8	12
Median	6.10×10^{-3}	6.57×10^{-4}	2.72×10^{-3}
		2.00×10^{-3}	

[a] In m/h.
[b] Outlier removed from further analysis.

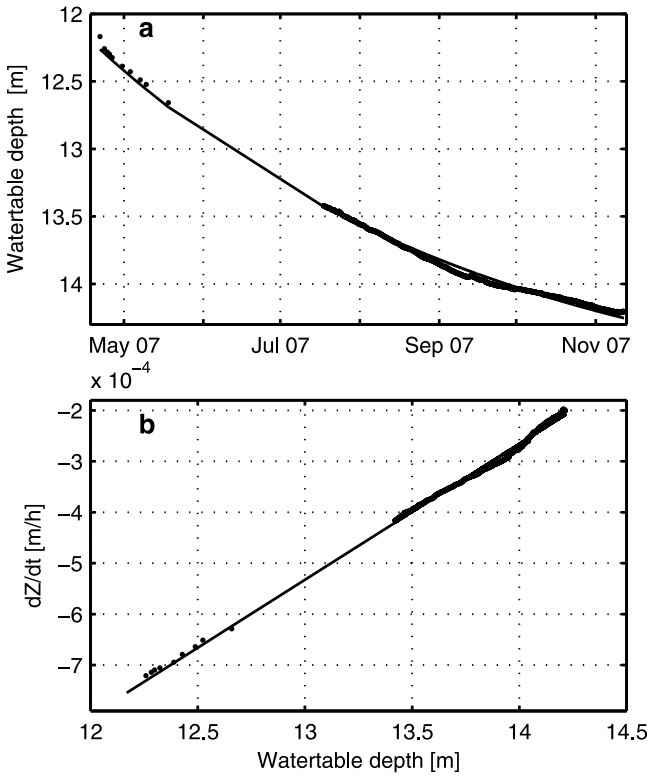

Figure 8. (a) Recession curve of the water table depth and (b) estimated Master Recession Curve.

to 173 mm. These values are in line with the estimated GW recharge of 130–190 mm/a for the area around the study area [*Apel et al.*, 1996] but lower than the groundwater recharge of 210–300 mm/a estimated by *Krásný and Sharp* [2007] for lower mountain ranges of the Bohemian Massif (mean annual precipitation of 800–1000 mm) and significantly lower than the estimated deep percolation rate of 909 mm/a in the study area of Markungsgraben in the National Park Bavarian Forest, which is ~50 km away [*Bittersohl et al.*, 2004]. This much higher percolation rate can be explained by higher annual precipitation of 1748 mm/a, but still more than half of the precipitation percolates deep into the ground. In this study, the deep percolation amounts to ~20% of the precipitation, which corresponds to the groundwater recharge rates estimated by *Krásný and Sharp* [2007] for Centro-European mountain ranges. Land use change or a high interflow rate could represent other explanations for the very high deep percolation rate of the Markungsgraben. *Haarhoff* [1989], for instance, estimated the groundwater recharge for the same area to be between 150 and 200 mm/a for a mean annual precipitation of 1000–1400 mm. Therefore, we must be aware that there may be a significant difference between deep percolation and groundwater recharge due to lateral fluxes in the soil or saprolite zone.

6.2. Groundwater Recharge

[34] The estimation of the lower boundary flux (the groundwater recharge q_R (m/h)) is based on the Water Table Fluctuation method (WTF) [*Healy and Cook*, 2002; *Sophocleous*, 1991] combined with the Master Recession Curve (MRC) [*Delin et al.*, 2007; *Heppner and Nimmo*, 2005], where the recharge is calculated as

$$q_R = S_Y \Delta Z_{WT} + q_D(Z_{WT}) \quad (6)$$

with ΔZ_{WT} being the water table rise (m) and $q_D(Z_{WT})$ being the groundwater discharge (m/h) at the corresponding water table depth. A characteristic water table decline hydrograph (an MRC) generally exists for each site. The MRC was developed by plotting the water table depth against the water table decline data for the period from 23 April 2007 to 5 November 2008 (Figure 8). By assuming that no groundwater recharge occurred during this period, we estimated the discharge by the following linear MRC

$$q_D(Z_{WT}) = S_Y(aZ_{WT} + b) \quad (7)$$

where a and b were estimated to be 0.002668 h^{-1} and −0.004001 m/h, respectively.

[35] Using the minimum, mean, and maximum specific yields (see Table 2) and the mean of both groundwater time series, we can estimate the cumulative groundwater recharge for the hydrological year of 2008 to be 50, 77, and 130 mm, respectively. These values are significantly lower than the estimated deep percolation and the cited groundwater recharge rates. The specific yield is estimated as a mean value over the whole aquifer thickness, but frequently, the specific yield decreases with increasing depth and so the specific yield in the zone where the groundwater fluctuation occurs may be underestimated. This might be reflected by the parameter S_Y being estimated from the snowmelt event, which corresponds to a groundwater recharge of 293 mm. In addition, only discharge in the groundwater zone is considered and interflow or saprolite flow are neglected. But interflow as well as the flow in the transition between fractured and weathered zone may be of major importance [*Cho et al.*, 2003].

6.3. Water Storage Change in the Saprolite Zone

[36] The deep percolation and groundwater recharge is highly dependent on the estimated K_s and S_Y, respectively [e.g., *Healy and Cook*, 2002; *Hubbell et al.*, 2004; *Nimmo et al.*, 1994; *Risser et al.*, 2009]. Here, we are interested in the seasonal WSC in the saprolite zone rather than in the absolute values of deep percolation and groundwater recharge. We will assume that on 1 November 2008, WSC in the saprolite zone are zero and that the cumulative q_P equals q_R. Because the estimated q_P is closer to the literature values than q_R, we will correct q_R to match q_P by using a S_Y of 0.024, which is in the estimated range of S_Y. Figure 9 shows the seasonal variation of cumulative deep percolation and groundwater recharge. The seasonal courses of both curves correspond well, with a time lag for the groundwater recharge compared to the deep percolation. At the end of February 2009, the cumulative groundwater recharge exceeded the cumulative deep percolation, something that is not physically possible. This effect is closely related to snowmelt (see Figure 3). During snowmelt, the soil is nearly saturated, which implies that preferential flow paths are activated and can contribute significantly to deep percolation [e.g., *French et al.*, 2002; *Stähli et al.*, 2004] and may even be intensified

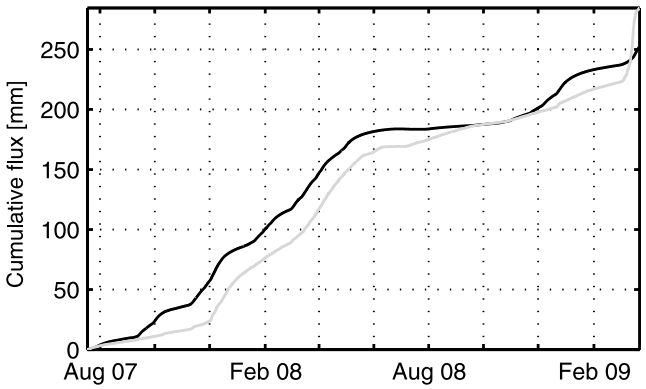

Figure 9. Seasonal variation of cumulative deep percolation (black line) and groundwater recharge (gray line).

by partly frozen soils [e.g., *Stähli et al.*, 1996]. As mentioned previously, preferential flow is not represented by the Buckingham-Darcy approach, which therefore fails under these conditions. As no correction was made here, this limitation has to be taken into account in the analysis of the saprolite gravity response.

[37] To assess the influence of the estimated van Genuchten parameters K_s and S_Y on the WSC in the saprolite zone, we calculated the deep percolation and the corresponding groundwater recharge for each of the four van Genuchten models and all measured K_s, with the prerequisite that the cumulative deep percolation cannot exceed the cumulative precipitation during the study period. These different realizations for each time step were used to calculate the minimum and maximum saprolite WSC.

7. Gravity and Water Storage Change

7.1. SG Residuals

[38] The major sources of temporal gravity variations are the tides of the solid Earth, ocean tide loading, and changes in the atmosphere and polar motion. These effects are modeled and removed from the signal after preprocessing of the raw data. The preprocessing comprises correction of the sensor's drift, signal conversion by a scale factor, and careful removal of spikes and disturbances (e.g., due to earthquakes). Scale factor and drift rate are reliably obtained by combining SG measurements with collocated absolute gravity measurements [*Wziontek et al.*, 2009a]. In this way, the scale factor is determined with a relative precision of better than 5 ppt. The almost linear instrumental drift of present SGs does not exceed 5.0 μGal/a, and the accuracy of its determination depends directly on the quality and repetition rate of the absolute gravity measurements. With two observation periods per year at the station Wettzell, the drift is determined with an accuracy of better than 0.5 μGal/a.

[39] The variation of the tidal potential due to Sun, Moon, and planets is described by precise tidal models [*Hartmann and Wenzel*, 1995; *Tamura*, 1987]. The elastic response of the solid Earth to the resulting forces is obtained by a harmonic analysis of the gravity signal up to monthly tides after atmospheric effects have been removed using a simple barometric admittance function. The effect of polar motion [*Wahr*, 1985] is calculated based on the pole coordinates as provided by the International Earth Rotation and Reference Systems Service (IERS) together with an adequate assumption of the elastic response of the Earth. We then performed a tidal analysis up to monthly tides. The accuracy of the SG residuals obtained can be estimated roughly with 0.1 μGal for short-term variations (1–30 days) and 0.5 μGal for interannual variations.

7.2. Gravity Response

[40] The gravity response of the different WSC is calculated based on the approach presented by *Creutzfeldt et al.* [2008] for a square with a side length of 4 km and the SG located in its center (Figure 1). We developed a spatially nested discretization domain and used the DEM to distribute the estimated WSC along the topography. The spatial resolution (Δxy = 0.25, 2.50, 10.00 m) of the DEM varies with the domain radius (R = 50, 500, 2000 m) (R: half the side length of the domain square). The z component of gravity change due to areal homogenous WSC is calculated for each body and time step using the MacMillan equation [*MacMillan*, 1958] presented by *Leirião et al.* [2009]

$$\Delta g = G\Delta\rho\Delta x\Delta y\Delta z\left[-\frac{z}{d^3}-\frac{5}{24}\frac{(\alpha x^2+\beta y^2+\omega z^2)z}{d^7}+\frac{1}{12}\frac{\omega z}{d^5}\right] \tag{8}$$

where $\alpha = 2\Delta x^2 - \Delta y^2 - \Delta z^2$, $\beta = -\Delta x^2 + 2\Delta y^2 - \Delta z^2$, $\omega = -\Delta x^2 - \Delta y^2 + 2\Delta z^2$ and $d = \sqrt{x^2+y^2+z^2}$. Variables x, y, and z are the center coordinates of an elementary body relative to the sensor (m). Δx, Δy, and Δz are the side lengths of a rectangular body ($\Delta xy = \Delta x = \Delta y$) (m), G is the gravitational constant (N m^2/kg^2), and $\Delta\rho$ is the density change in an elementary body (kg/m^3), which is directly related to the WSC. The total hydrological gravity effect (the gravity response) is derived by the summation of all gravity changes in each elementary body caused by the estimated water mass changes in the model domain.

[41] The SG building has a significant influence on the gravity response [*Creutzfeldt et al.*, 2008]. We assume that neither in the foundation nor in the base plate of the SG building WSC occur. When taking into account the umbrella effect of the SG building inhibiting infiltration of rainfall into the soil, no WSC occur below the base plate of the SG building in the topsoil storage. For the soil storage, we calculated the average gravity response both for cases excluding and including mass variations below the base plate. Snow accumulates on the roof of the SG building, and precipitation that runs off the roof is routed away from the SG. Therefore, the effect of water redistribution from the roof to the tank is not accounted for.

[42] For each water storage component, namely snow, topsoil zone, soil zone, saprolite zone, and groundwater storage, the respective relative gravity response was calculated independently, using 18 July 2007 as the reference date (Figure 10). As a measure of uncertainty for water storage, we calculated the minimum, mean, and maximum WSC for the upper soil and the soil storage for each time step, based on the data of all available soil moisture probes. The minimum, mean, and maximum saprolite zone WSC were derived as described in section 6. The minimum, mean, and maximum groundwater gravity responses were derived

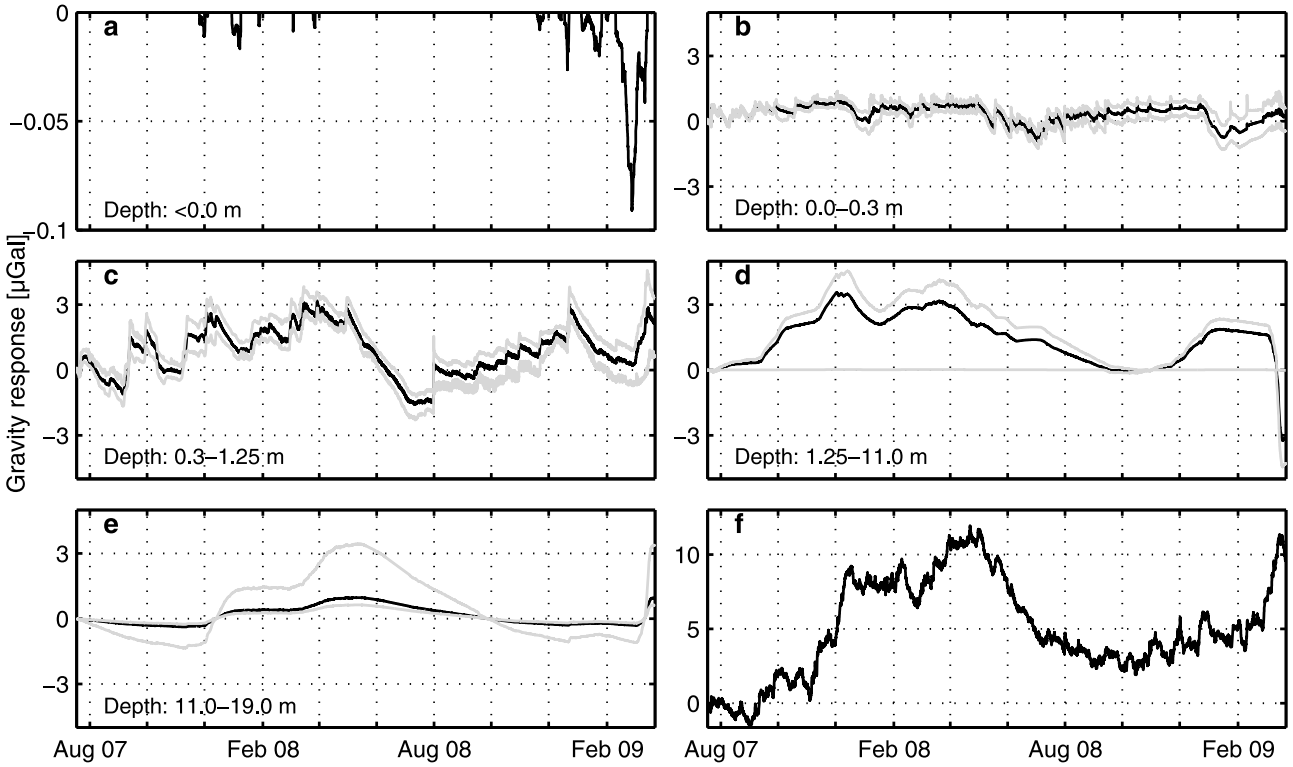

Figure 10. Temporal changes of mean gravity response (black line) due to WSC in (a) the snow layer, (b) the topsoil zone, (c) the soil zone, (d) the saprolite zone, and (e) the groundwater storage and (f) the measured SG residuals. Gray lines are the estimated minimum and maximum gravity response.

using the specific yields 6.30×10^{-3}, 9.61×10^{-3}, and 3.41×10^{-2}, respectively, and the mean water table depth, which was corrected for the pump test. Finally, we estimated the total minimum, mean, and maximum gravity response by summing up the minimum, mean, and maximum gravity response for each time step independently.

[43] Figure 10 shows the gravity response of the different water storage components. Except for snow, the gravity response of all other components is of the same order of magnitude. The gravity response of the snow storage is negative, because snow mass accumulates mainly above the SG sensor in its immediate vicinity. At larger distances, snow also accumulates below the SG sensor so that the snow masses compensate each other and the gravity response of snow becomes negligible. Nonetheless, as pointed out in the previous sections, snow is an important factor as it significantly influences the other storage components via flow processes driven by snowmelt.

[44] Storage change in the topsoil and the resulting gravity response are generally closely related to precipitation and do not show pronounced seasonal dynamics. During winter, the apparent decline of the gravity response for both soil storages is not only due to a change of soil moisture but due to the change of permittivity caused by the soil freezing, as explained above.

[45] WSC time series in the soil, in the saprolite, and in the groundwater zone exhibit a similar seasonal pattern. As discussed in section 7.1, the overall deep percolation might be underestimated with the present approach. This could cause an underestimation of the saprolite storage influence on the total gravity response. The sharp decline of the gravity response in the saprolite zone at the end of the study period is most likely due to methodological reasons because the effect of macropores is considered only at the lower boundary, as explained in section 6.

7.3. Comparison of Gravity Response and SG Residuals

[46] Figure 10 shows the gravity response of the different water storage components compared with the SG residuals. The time series of deeper WSC components such as groundwater, saprolite, and soil storage show a similar seasonal behavior as the SG residuals, something which is also expressed by high correlation coefficients (Table 5). The highest correlation, however, was found for the gravity response integrated over all storage components.

[47] However, single hydrological state variables also show a significantly high correlation with the SG residuals. For example, the correlation coefficients between the time

Table 5. Correlation Coefficient Between Time Series of Water Storage Components and the SG Residuals[a]

	Mean	Max.	Min.
Snow	−0.09	–	–
Top soil storage	0.09	0.25	−0.01
Soil storage	0.64	0.65	0.61
Saprolite storage	0.49	0.64	−0.18
Groundwater storage	0.71	0.73	0.62
Total storage	0.73	0.88	0.61

[a]Mean, max., and min. are the gravity responses due to the mean, maximum, and minimum estimated WSC, respectively.

Table 6. Regression Coefficient, Standard Error, *t* Value, *p* Value, and Performance Criteria of the Multiple Linear Regression Model for Time Series of SG Residuals and the Gravity Response of the Different Water Storages for the Entire Study Period[a]

Variable	Regression Coefficient	Standard Error	*t*	*p*
Intercept	2.42	0.02	145.10	<0.001
Groundwater storage	5.02	0.02	208.00	<0.001
Soil storage	1.56	0.01	137.80	<0.001
Saprolite storage	0.43	0.01	46.23	<0.001
Top soil storage	−0.58	0.03	−19.86	<0.001
Snow	−71.17	0.96	−73.92	<0.001

[a]Standard deviation of error: 1.135. Multiple R^2: 0.88. *F* statistic 21544 on 5 and 14748 degrees of freedom, *p* value: 0.

series of two TDR soil moisture measurements in 2 m depth and the SG residuals are 0.65 and 0.79 (see also Figure 4f and 10f). Focusing on the relationship between SG residuals and groundwater level alone would result in a regression coefficient of 2.69 μGal gravity response per meter groundwater change (coefficient of determination = 0.51). On the basis of the Bouguer slab approximation, where a 1 m water change in an infinitely extended slab causes a gravity change of 41.92 μGal, this regression slope corresponds to a specific yield of 6.42×10^{-2}. *Harnisch and Harnisch* [2006, 2002] estimated the regression coefficient as being in the range of 2.48 and 9.33 μGal/m based on a groundwater well at a distance of 200 m to the SG. This would result in a specific yield between 5.91×10^{-2} and 2.23×10^{-1}. As they already pointed out, interpreting this regression coefficient in a physical way is problematic and only valid if the correlation between groundwater and other water storages can be neglected or the water mass variations in all other storages are small compared to the groundwater mass variation.

[48] These assumptions are not fulfilled for the Wettzell site. Strong interaction between different water storages exists and the SG residuals depend on different WSC components. For example, a rise of the groundwater level occurs after accumulation of water in the vadose zone or melting of the snow water. A multiple linear regression showed that all variables have a statistically significant predictive capability for SG residuals ($p < 0.001$). The development of the model was studied by including/excluding different WSC components step by step. Finally, variables were included in the model step by step to explain as much of the variability as possible in each individual step. Studying the step-by-step development of the statistical model, groundwater explains 51% of the variability in the SG residuals' time series. By including soil moisture in the model, the coefficient of determination increased to 0.80. Upon adding the saprolite zone storage and the topsoil zone storage, the coefficient of determination was estimated to be 0.82 and 0.83, respectively. Finally, the coefficient of determination increased to 0.88 upon inclusion of the snow storage. The parameters of the final model are shown in Table 6. While snow came out as the third most important component in terms of explained variability, it was placed in the last position, because here it compensates for the methodological shortcomings of estimating the saprolite storage change (March 2009), which is also reflected by a large negative regression coefficient (Table 6).

[49] Despite the high coefficient of determination, the total estimated mean gravity response is smaller than the SG residuals. This is also reflected in Figure 12, where the total gravity response of all different water storages is compared to the SG residuals together with the minimum and maximum gravity response for each time step as a measure of uncertainty as explained above. For the study period, the range of minimum and maximum estimated gravity response amounts to 14 μGal. This value is very similar to the range of the observed SG residuals. Given that a water mass change of 1 m amounts to a gravity response of 52 μGal (due to topography) [*Creutzfeldt et al.*, 2008], the gravity range of 14 μGal corresponds to a total water storage change of 272 mm around the gravimeter between the driest and wettest conditions recorded in the observation period.

[50] The time series of total WSC and SG residuals exhibit similar dynamics both at the seasonal scale and for individual periods or events. Short peaks related to discrete rainfall correspond well in time (for example, during the recession period from May to July 2008), whereas differences exist in the absolute value, e.g., the gravity increase for the largest rainfall event on 31 July 2008 is higher for the gravity response (1.9–2.9 μGal) than for the SG residuals (1.4 μGal). The seasonal correlation of the curves is expressed by a correlation coefficient ranging from 0.61 to 0.88 (Table 5). The maximum gravity response estimated based on the assumed uncertainty of the observation data correlates better with the SG residuals than the mean or the minimum gravity response (Figure 12). One possible explanation is that local WSC have been underestimated by the hydrological methods. As another explanation, the parts of the differences between the estimated gravity response and the SG residuals may be due to the effect of large-scale hydrological variations when assuming a strong correlation between the local and large-scale WSC. As shown by *Wziontek et al.* [2009b], most of the hydrological large-scale effect is generated in a zone with a radius of 200 km up to 10,000 km around the SG and may amount to a few μGal. Nevertheless, it cannot be expected that large-scale variations will significantly contribute to the event-scale variations of the SG signal. For example, the steep rise of the SG residuals by about 6 μGal from 27 February to 20 March 2009 was most likely caused by local WSC due to the snowmelt and water mass redistribution in the soil. This provides additional evidence that the local gravity response tends to be underestimated.

[51] An analysis of the SG residuals during the pump test reveals that the SG residuals do not show a clear correlation with the groundwater table displacement. In the beginning, a gravity rise of ~0.2 μGal can be observed, followed by a decline of ~0.4 μGal and another rise of ~0.4 μGal (Figure 11). This ambivalent response of the SG residuals is difficult to interpret because the gravity response depends on the specific yield as well as on the hydraulic conductivity of the aquifer as pointed out by *Blainey et al.* [2007]. In general, the results support that the drainable porosity is small, but it is not possible to draw the conclusion that the overall gravity effect of groundwater table variations is negligible because the water level depression cone is of limited spatial extent causing water mass variations that have barely any gravity effect for this specific case. Also *Harnisch and Harnisch* [2006, 2002] did not find a clear relation for a pump test conducted at a distance of 250 m. They observed a decline of 1 μGal in the SG residuals with

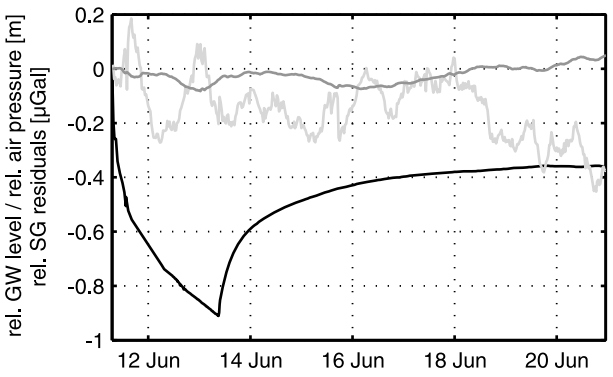

Figure 11. Time series during pump test of corrected relative groundwater displacement in meters (black line), relative SG residuals in μGal (light gray line), and relative air pressure in meter of water (gray line).

a time lag of 12 h and assumed this decline to be caused by the groundwater displacement.

8. Discussion

[52] As illustrated in Figures 10 and 12, the estimation of local WSC and of its gravity response are associated with considerable uncertainties. This study considers only specific aspects within a broad set of uncertainties in both hydrological and gravimetric procedures: (1) measurement accuracy (sensor calibration, resolution of device, etc.), (2) assumptions and simplifications in the structural model of the subsurface, (3) hydro(geo)logical parameter estimation, (4) spatial variability, (5) calculation of the gravity response (impact of, e.g., topography and SG building), and (6) processing of the SG residuals.

[53] Points 2–5 are the most critical aspects in this study. Errors in representing hydrological processes are mainly associated with the saprolite zone, because only matric flow is considered, neglecting preferential flow as well as lateral fluxes in the saprolite or the periglacial weathering cover. For the estimation of fluxes in the saprolite zone, data from different sources (TDR probes, tensiometers, pressure transducer) correspond well in terms of their seasonal variations, but the quantification of total WSC in the saprolite zone is associated with a high level of uncertainty. The estimation of effective soil hydraulic parameters as well as aquifer parameters is still a challenging task.

[54] Concerning spatial variability, Figures 4, 5, and 10 and Table 1 provide preliminary evidence that supports the validity of the 1-D approach adopted in this study because heterogeneity is much more pronounced with depth than with area, especially when considering the near-field effect of local WSC on the SG residuals. However, the spatial variability at larger distances along the hillslope with potentially different soil moisture and groundwater regimes is not considered here. In addition, the soil moisture dynamics below the SG building are not known exactly, even though this zone has a high influence on the SG measurements.

[55] The uncertainties arising from the estimation of WSC on the local scale by classical hydrological methods point to the potential use of precise temporal gravity measurements in hydrology. In general, the advantage as well as disadvantage of gravity measurements is their integrative character. On the one hand, this makes them capable of integrating a small catchment-scale hydrological response, similar in nature to discharge measurements [*Hasan et al.*, 2008]. Thus, they might be especially useful in areas far away from the river such as headwaters, where no adequate

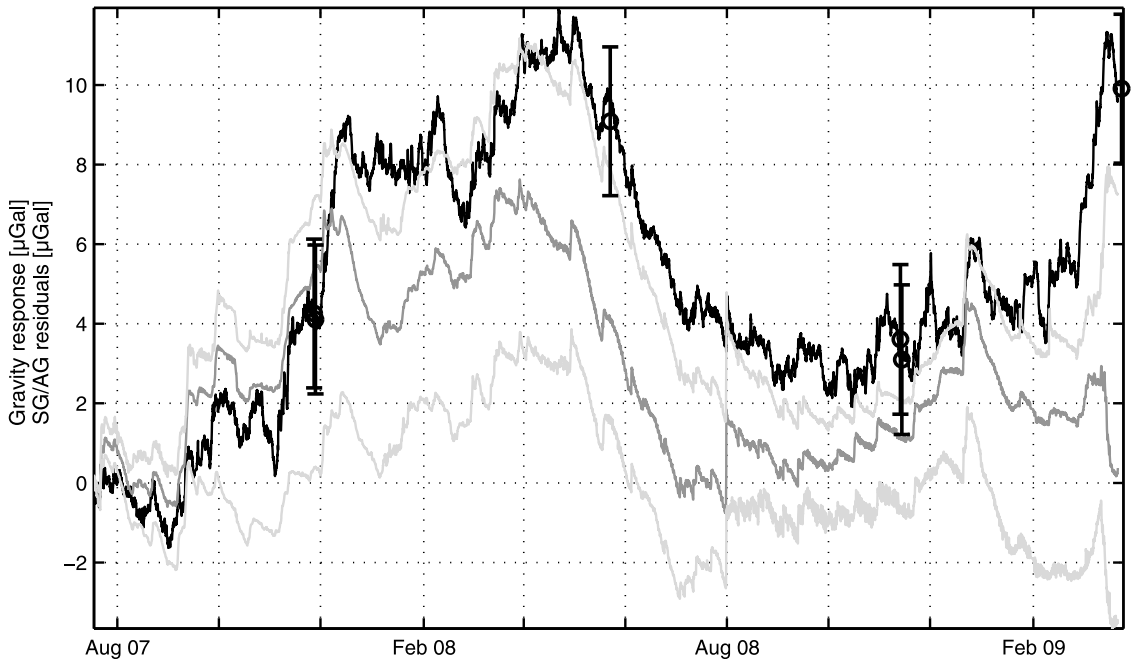

Figure 12. SG residuals (black line) and total gravity response as sum of all water storage components (dark gray line). Light gray lines are the minimum and maximum estimated gravity response. Absolute gravity (AG) residuals and their uncertainty are displayed as circles with error bars.

measurement technique is available to estimate local WSC and integrative catchment dynamics. In this study, for example, we assume that, over a 1 year period, the WSC in the saprolite zone are zero. However, the positive trend of the SG residuals compared to the total hydrological gravity response may be an indication that water accumulates over this period in the saprolite zone. On the other hand, due to the integrative character of gravity measurements, it is difficult to unambiguously identify the source of the gravimeter signal. This makes a unique interpretation for individual storage components challenging or even impossible if no complementary information is available.

[56] Favourable conditions for a hydrological interpretation of gravimetric data prevail where WSC occur either above or below the gravimeter. This applies to the gravimeter in Wettzell, where most of the WSC occur below the gravimeter. This is in contrast to SGs installed at underground locations where local water storage may change above and below the gravimeter so that local WSC may compensate for each other to some extent in the gravimeter signal. This may imply that large-scale WSC make a relatively larger contribution to the SG signal. Additionally, in the direct surroundings of the SG, the hydrological system should be kept as simple as possible, (i.e., avoiding stone or Earth cover or artificial drainage systems close to the gravimeter that are difficult to interpret). The uncertainties discussed above indicate that it may be difficult to completely remove the local hydrological effect from gravity data (i.e., providing SG residuals that are free from local "hydrological noise" and that could be used for geodetic and large-scale applications such as validation of satellite gravity data [e.g., *Weise et al.*, 2009] or of large-scale hydrological models).

[57] In view of the potential applications and limitations of gravity measurements and toward a broader evaluation of their value for hydrological applications, further research is needed on quantifying hydrological processes and state variables including their spatial variability around SGs. At the Wettzell site, studies using additional soil moisture and groundwater sensors, a lysimeter, tracer tests, permanent electrical resistivity (ERT) surveys, and a second SG are under progress to better describe processes such as evapotranspiration, deep percolation, preferential or saprolite flow, and their relation to gravity data. The evaluation will benefit by combining hydrological and geophysical data in a joint or coupled hydrogeophysical inversion [*Ferré et al.*, 2009], whereas spatial gravity changes caused by WSC can be resolved by repeated observations with relative gravimeters [*Naujoks et al.*, 2008]. Finally, we also suggest performing detailed hydrological analyses of all relevant water storage components at other SG stations in order to extend the evaluation and learn from different environmental settings.

9. Conclusions

[58] In this study, we present a comprehensive observation-based approach for the estimation of total local water storage, composed of the components snow, soil moisture, saprolite, and groundwater storage. Continuous time series of WSC in each component were estimated, including their possible range of uncertainty by minimum and maximum storage values. Nevertheless, not all sources of uncertainty could be addressed in this study.

[59] For each storage component, the gravity response was calculated considering the spatial distribution of water masses around the SG. The results were compared to the SG gravity observations. Except for the small effect of the snow storage, the gravity response of the different storage components is of the same order of magnitude. A linear regression model showed that all storage changes estimated from hydrological observations have a significant predictive capability for the SG gravity signal. Some hydrological state variables as well as single-storage components correlate well with the SG residuals. However, a strong correlation does not necessarily imply a physical relation (direct effect of water masses on the SG) but may indicate only that a particular observable variable is a reasonable indicator for part of the storage changes in the area surrounding the SG.

[60] Comparing the total gravity response of the WSC to the SG residuals shows similarities on the event scale as well as on the seasonal time scale. A large part of the gravity signal can be explained by local WSC. An uncertainty analysis based on the observation data showed that the maximum gravity response correlates better with the SG residuals than the mean or the minimum estimated gravity response. Therefore, we argue that the local hydrological gravity effect tends to be underestimated in this study, since large-scale hydrological mass variations can contribute only a few μGal on the seasonal time scale to the total gravity signal.

[61] Estimating local WSC is associated with uncertainties (measurement errors, model assumptions, parameter estimation, process quantification, and spatial variability) and demonstrates the limitations of conventional hydrological instruments to quantify local WSC. This demonstrates the shortcomings of providing a gravity signal free of local "hydrological noise." It highlights that the signal separation process is an iterative process and that different disciplines have to work together closely.

[62] The disadvantage as well as the advantage of gravity measurements is their integrative nature. It makes gravity observation difficult to interpret, and therefore, extreme caution should be applied when interpreting a gravity signal for hydrological studies, especially if only a single parameter or a single water storage component is studied. Nevertheless, gravity measurements can provide unique data for hydrological studies and thus have a high potential to improve water balance studies and catchment characterization by estimating the storage term, for example, in order to set up storage-discharge functions [*Kirchner*, 2009].

[63] **Acknowledgments.** This work has been supported by the Deutsche Forschungsgemeinschaft (German Research Foundation) within the Priority Program SPP 1257 "Mass transport and mass distribution in the system Earth," project TASMAGOG. We want to thank the editor John Selker, the associate editor Frederick Day-Lewis, the reviewer Ty Ferré, the reviewer Michel Van Camp, and one anonymous reviewer for the thoughtful comments that significantly improved the study.

References

Apel, R., A. Klemm, and F. Rüdiger (1996), Grundlagen zum Wasserwirtschaftlichen Rahmenplan Naab-Regen. Hydrogeologie, Bayerisches Geologisches Landesamt, München.

Bittersohl, J., K. Moritz, C. Schöttl, and H. Wahler (2004), *15 Jahre Integriertes Messnetz: Stoffeintrag – Grundwasser, Methoden und Ergebnisse*, Bayerisches Landesamt für Wasserwirtschaft München.

BKG (2005), ATKIS® Basis-DLM, edited, © Vermessungsverwaltungen der Länder und BKG (Bundesamt für Kartographie und Geodäsie).

Blainey, J. B., T. P. A. Ferré, and J. T. Cordova (2007), Assessing the likely value of gravity and drawdown measurements to constrain estimates of hydraulic conductivity and specific yield during unconfined aquifer testing, *Water Resour. Res.*, *43*, W12408, doi:10.1029/2006WR005678.

Bower, D. R., and N. Courtier (1998), Precipitation effects on gravity measurements at the Canadian Absolute Gravity Site, *Phys. Earth Planet. In.*, *106*(3–4), 353–369.

Buckingham, E. (1907), Studies in the movement of soil moisture, Bulletin 38, U.S. Department of Agriculture, Bureau of Soils, Washington D. C.

Büttner, G., R. Pamer, and B. Wagner (2003), Hydrogeologische Raumgliederung von Bayern, Bayerisches Geologisches Landesamt, München.

Campbell Scientific Inc. (2008), TDR100: Manual, Campbell Scientific Inc., Logan, USA.

Campbell Scientific Inc. (2009), CR1000 Measurement and Control System: Manual, Campbell Scientific Inc., Logan, USA.

Cho, M., Y. Choi, K. Ha, W. Kee, P. Lachassagne, and R. Wyns (2003), Relationship between the permeability of hard rock aquifers and their weathering, from geological and hydrogeological observations in South Korea, paper presented at International Association of Hydrogeologists IAH Conference on "Groundwater in fractured rocks," Prague.

Cooper, H. H., and C. E. Jacob (1946), A generalized graphical method for evaluating formation constants and summarizing well field history, *Trans. Am. Geophys. Union*, *27*(4), 526–534.

Creutzfeldt, B., A. Guntner, T. Klugel, and H. Wziontek (2008), Simulating the influence of water storage changes on the superconducting gravimeter of the Geodetic Observatory Wettzell, Germany, *Geophysics*, *73*, WA95.

Crossley, D., S. Xu, and T. v. Dam (1998), Comprehensive analysis of 2 years of SG data from Table Mountain, Colorado, in *13th International Symposium on Earth Tides*, edited, Observatoire Royal de Belgique, Brussels.

Crossley, D., J. Hinderer, M. Llubes, and N. Florsch (2003), The potential of ground gravity measurements to validate GRACE data, *Adv. Geosci.*, *1*, 65–71.

Delin, G. N., R. W. Healy, D. L. Lorenz, and J. R. Nimmo (2007), Comparison of local- to regional-scale estimates of ground-water recharge in Minnesota, USA, *J. Hydrol.*, *334*, 231–249.

DIN (1998), *Pedologic site assessment – Designation, classification and deduction of soil parameters (normative and nominal scaling)*, Deutsches Institut für Normung, Berlin.

Ferré, T. P. A., L. Bentley, A. Binley, N. Linde, A. Kemna, K. Singha, K. Holliger, J. A. Huisman, and B. Minsley (2009), Critical steps for the continuing advancement of hydrogeophysics, *Eos. Trans. AGU*, *90*.

French, H. K., C. Hardbattle, A. Binley, P. Winship, and L. Jakobsen (2002), Monitoring snowmelt induced unsaturated flow and transport using electrical resistivity tomography, *J. Hydrol.*, *267*(3–4), 273–284.

Gehman, C. L., D. L. Harry, W. E. Sanford, J. D. Stedick, and N. A. Beckman (2008), Estimating specific yield and storage change in an unconfined aquifer using temporal gravity surveys, *Water Resour. Res.*, *45*, W00D21, doi:10.1029/2007WR006096.

Gettings, P., D. S. Chapman, and R. Allis (2008), Techniques, analysis, and noise in a Salt Lake Valley 4D gravity experiment, *Geophysics*, *73*, WA71, doi:10.1190/1.2996303.

Haarhoff, T. (1989), The effect of acid rain and forest die-back on groundwater – case studies in Bavaria, Germany (FRG), paper presented at Atmospheric Deposition. Proceedings of a Symposium held during the Third Scientific Assembly of the International Association of Hydrological Sciences, IAHS, Baltimore, Maryland.

Harnisch, G., and M. Harnisch (2006), Hydrological influences in long gravimetric data series, *J. Geodyn.*, *41*, 276–287.

Harnisch, M., and G. Harnisch (2002), Seasonal variations of hydrological influences on gravity measurements at Wettzell, *Bulletin d'Information des Marées Terrestres*, *137*, 10,849–10,861.

Hartmann, T., and H. G. Wenzel (1995), Catalogue HW95 of the tide generating potential, *Bulletin d'Information des Marées Terrestres*, *123*, 9278–9301.

Hasan, S., P. A. Troch, P. W. Bogaart, and C. Kroner (2008), Evaluating catchment-scale hydrological modeling by means of terrestrial gravity observations, *Water Resour. Res.*, *44*, W08416, doi:10.1029/2007WR006321.

Haude, W. (1955), Zur Bestimmung der Verdunstung auf möglichst einfache Weise, Deutscher Wetterdienst, Bad Kissingen.

Healy, R., and P. Cook (2002), Using groundwater levels to estimate recharge, *Hydrogeol. J.*, *10*(1), 91–109.

Heppner, C. S., and J. R. Nimmo (2005), A computer program for predicting recharge with a Master Recession Curve, U.S. Geological Survey, Washington, USA.

Hohmann, M. (1997), Soil freezing – The concept of soil water potential. State of the art, *Cold Reg. Sci. Technol.*, *25*(2), 101–110.

Hokkanen, T., K. Korhonen, and H. Virtanen (2006), Hydrogeological effects on superconducting gravimeter measurements at Metsähovi in Finland, *J. Environ. Eng. Geophys.*, *11*, 261–267.

Hubbell, J. M., M. J. Nicholl, J. B. Sisson, and D. L. McElroy (2004), Application of a Darcian approach to estimate liquid flux in a deep vadose zone, *Vadose Zone J.*, *3*, 560–569.

Jacob, C. E. (1944), Notes on determining permeability by pumping tests under watertable conditions, U.S. Geological Survey, Washington, USA.

Jacob, T., R. Bayer, J. Chery, H. Jourde, N. L. Moigne, J.-P. Boy, J. Hinderer, B. Luck, and P. Brunet (2008), Absolute gravity monitoring of water storage variation in a karst aquifer on the larzac plateau (Southern France), *J. Hydrol.*, *359*, 105–117.

Jacob, T., J. Chery, R. Bayer, N. L. Moigne, J.-P. Boy, P. Vernant, and F. Boudin (2009), Time-lapse surface to depth gravity measurements on a karst system reveal the dominant role of the epikarst as a water storage entity, *Geophys. J. Int.*, *17*, 347–360.

Kirchner, J. W. (2009), Catchments as simple dynamical systems: Catchment characterization, rainfall-runoff modeling, and doing hydrology backward, *Water Resour. Res.*, *45*, W02429, doi:10.1029/2008WR006912.

Krásný, J., and J. M. Sharp (2007), Hydrogeology of fractured rocks from particular fractures to regional approaches: State-of-the-art and future challenges, in *Groundwater in Fractured Rocks*, edited by J. Krásný and J. M. Sharp, Routledge, Prague.

Kruseman, G. P., and N. A. de Ridder (1990), *Analysis and Evaluation of Pumping Test Data*, 2nd (completely revised) ed., International Institute for Land Reclamation and Improvement, Wageningen.

Langguth, H.-R., and R. Voigt (1980), *Hydrogeologische Methoden*, 2. überarbeitete und erweiterte Auflage ed., Springer-Verlag, Berlin.

Leirião, S., X. He, L. Christiansen, O. B. Andersen, and P. Bauer-Gottwein (2009), Calculation of the temporal gravity variation from spatially variable water storage change in soils and aquifers, *J. Hydrol.*, *365*, 302–309.

LfL (2009), Agrarmeteorologisches Messnetz Bayern: Wetterstation Nr.127, Allmannsdorf, Bayerische Landesanstalt für Landwirtschaft (Bavarian State Research Center for Agriculture) (LfL), Freising-Weihenstephan, Germany.

Llubes, M., N. Florsch, J. Hinderer, L. Longuevergne, and M. Amalvict (2004), Local hydrology, the Global Geodynamics Project and CHAMP/GRACE perspective: some case studies, *J. Geodyn.*, *38*, 355–374.

MacMillan, W. D. (1958), *Theoretical Mechanics: The Theory of the Potential*, Dover Publications, Inc., New York.

Maréchal, J. C., B. Dewandel, and K. Subrahmanyam (2004), Use of hydraulic tests at different scales to characterize fracture network properties in the weathered-fractured layer of a hard rock aquifer, *Water Resour. Res.*, *40*, W11508, doi:10.1029/2004WR003137.

Mualem, Y. (1976), A new model for predicting the hydraulic conductivity of unsaturated porous media, *Water Resour. Res.*, *12*(3), 513–522, doi:10.1029/WR012i003p00513.

Naujoks, M., A. Weise, C. Kroner, and T. Jahr (2008), Detection of small hydrological variations in gravity by repeated observations with relative gravimeters, *J. Geodesy*, *82*, 543–553.

Naujoks, M., C. Kroner, A. Weise, T. Jahr, P. Krause, and S. Eisner (2010), Evaluating local hydrological modelling by temporal gravity observations and a gravimetric three-dimensional model, *Geophys. J. Int.*, *182*(1), 233–249.

Neumeyer, J., F. Barthelmes, C. Kroner, S. Petrovic, R. Schmidt, H. Virtanen, and H. Wilmes (2008), Analysis of gravity field variations derived from superconducting gravimeter recordings, the GRACE satellite and hydrological models at selected European sites, *Earth Planets Space*, *60*, 505–518.

Nimmo, J. R., D. A. Stonestrom, and K. C. Akstin (1994), The feasibility of recharge rate determinations using the steady-state centrifuge method, *Soil Sci. Soc. Am. J.*, *58*(1), 49–56.

Pool, D. R. (2008), The utility of gravity and water-level monitoring at alluvial aquifer wells in southern Arizona, *Geophysics*, *73*, WA49, doi:10.1190/1.2980395.

Pool, D. R., and J. H. Eychaner (1995), Measurements of aquifer-storage change and specific yield using gravity surveys, *Ground Water*, *33*(3), 425–432.

Raum, K. D. (2002), Markierungstechnische bruchtektonisch-gefügekundliche und fotogeologische Untersuchungen zur Ermittlung der Grundwasserfließverhältnisse in der Verwitterungszone kristalliner Gesteine in Quellgebieten des Oberpfälzer/Bayerischen Waldes (Ost-Bayern/Deutschland), 1–242 pp, Friedrich-Alexander-Universität, Erlangen-Nürnberg.

Risser, D., W. Gburek, and G. Folmar (2009), Comparison of recharge estimates at a small watershed in east-central Pennsylvania, USA, *Hydrogeol. J.*, *17*, 287–298.

Roth, C., M. Malicki, and R. Plagge (1992), Empirical evaluation of the relationship between soil dielectric constant and volumetric water content as the basis for calibrating soil moisture measurements by TDR, *J. Soil Sci.*, *43*(1), 1–13.

Rubbert, T. K. (2008), Hydrogeologische Modellbildung eines kombinierten porös-geklüfteten Grundwasserleitersystems des Bayerischen Waldes, Ruhr-Universität, Bochum.

Schlüter, W., N. Brandl, R. Dassing, H. Hase, T. Klügel, R. Kilger, P. Lauber, A. Neidhardt, C. Plötz, S. Riepl, and U. Schreiber (2007), Fundamentalstation Wettzell - ein geodätisches Observatorium, *Zeitschrift für Vermessungswesen*, *132*, 158–167.

SEBA (2008), Data Logger MDS Dipper-TEC: Water Level, Temperature, Electrical Conductivity, SEBA Hydrometrie GmbH, Kaufbeuren, Germany.

Sommer (2007), Snow pillow 3 × 3 m, Sommer GmbH & Co KG, Koblach, Austria.

Sommer (2008), USH-8: Ultrasonic Snow Depth Sensor, Sommer GmbH & Co KG, Koblach, Austria.

Sophocleous, M. A. (1991), Combining the soilwater balance and water-level fluctuation methods to estimate natural groundwater recharge: Practical aspects, *J. Hydrol.*, *124*(3–4), 229–241.

Stähli, M., P.-E. Jansson, and L.-C. Lundin (1996), Preferential water flow in a frozen soil – a two-domain model approach, *Hydrol Process*, *10*(10), 1305–1316.

Stähli, M., D. Bayard, H. Wydler, and H. Flühler (2004), Snowmelt infiltration into alpine soils visualized by dye tracer technique, *Arct. Antarct. Alp. Res.*, *36*, 128–135.

Tamura, Y. (1987), A harmonic development of the tide-generating potential, *Bulletin d'Information des Marées Terrestres*, *99*, 6813–6855.

TGL (1974), 23864/02-10 Hydrogeologie, Amt für Standardisierung, Messwesen und Warenprüfung der DDR (ASMW), Berlin, Germany.

Theis, C. V. (1935), The relation between the lowering of the piezometric surface and the rate and duration of discharge of a well using groundwater storage, *Trans. Am. Geophys. Union*, *16*, 519–524.

Topp, G. C., J. L. Davis, and A. P. Annan (1980), Electromagnetic determination of soil water content: measurements in coaxial transmission lines, *Water Resour. Res.*, *16*(3), 574–582, doi:10.1029/WR016i003p00574.

Van Camp, M., M. Vanclooster, O. Crommen, T. Petermans, K. Verbeeck, B. Meurers, T. v. Dam, and A. Dassargues (2006), Hydrogeological investigations at the Membach station, Belgium, and application to correct long periodic gravity variations, *J. Geophys. Res.*, *111*, B10403, doi:10.1029/2006JB004405.

van Genuchten, M. T. (1980), A closed-form equation for predicting the hydraulic conductivity of unsaturated soils, *Soil Sci. Soc. Am. J.*, *44*(5), 892–898.

Virtanen, H. (2001), Hydrological studies at the Gravity Station Metasahovi in Finland, *J. Geodetic Soc. Jpn.*, *47*(1), 328–333.

Völkel, J. (1995), Periglaziale Deckschichten und Böden im Bayerischen Wald und seinen Randgebieten als geogene Grundlagen landschaftsökologischer Forschung im Bereich naturnaher Waldstandorte, *Z. Geomorphol.*, *96*.

Wahr, J. M. (1985), Deformation induced by polar motion, *J. Geophys. Res.*, *90*(B11), 9363–9368, doi:10.1029/JB090iB11p09363.

Weise, A., C. Kroner, M. Abe, J. Ihde, G. Jentzsch, M. Naujoks, H. Wilmes, and H. Wziontek (2009), Terrestrial gravity observations with superconducting gravimeters for validation of satellite-derived (GRACE) gravity variations., *J. Geodyn.*, *48*(3–5), 325–330.

Werth, S., A. Güntner, S. Petrovic, and R. Schmidt (2009), Integration of GRACE mass variations into a global hydrological model, *Earth Planet. Sci. Lett.*, *277*, 166–173.

Wziontek, H., R. Falk, H. Wilmes, and P. Wolf (2009a), Precise gravity time series and instrumental properties from combination of superconducting and absolute gravity measurements, in *Observing our Changing Earth*, edited by M. G. Sideris, pp. 301–306.

Wziontek, H., H. Wilmes, P. Wolf, S. Werth, and A. Güntner (2009b), Time series of superconducting gravimeters and water storage variations from the global hydrology model WGHM, *J. Geodyn.*, *48*(3–5), 166–171.

B. Creutzfeldt, A. Güntner, B. Merz, and H. Thoss, Section of Hydrology, German Research Centre for Geosciences, Potsdam, Germany. (benjamin.creutzfeldt@gfz-potsdam.de; andreas.guentner@gfz-potsdam.de; bruno.merz@gfz-potsdam.de; heiko.thoss@gfz-potsdam.de)

H. Wziontek, Section of National Reference Systems for Gravity, Federal Agency for Cartography and Geodesy, Frankfurt, Germany. (hartmut.wziontek@bkg.bund.de)